


## RESEARCH ARTICLE

# Linking bioenergetic function of mitochondria to tissue-specific molecular fingerprints

 Lisa Kappler,<sup>1</sup> Miriam Hoene,<sup>1</sup> Chunxiu Hu,<sup>2</sup> Christine von Toerne,<sup>3</sup> Jia Li,<sup>1,4</sup> Daniel Bleher,<sup>1</sup> Christoph Hoffmann,<sup>1</sup> Anja Böhm,<sup>5,6</sup> Laxmikanth Kollipara,<sup>7</sup> Hans Zischka,<sup>8,9</sup> Alfred Königsrainer,<sup>10,11</sup> Hans-Ulrich Häring,<sup>1,5,6</sup> Andreas Peter,<sup>1,5,6</sup> Guowang Xu,<sup>2</sup> Albert Sickmann,<sup>7,12,13</sup> Stefanie M. Hauck,<sup>3,6</sup> Cora Weigert,<sup>1,5,6</sup> and Rainer Lehmann<sup>1,5,6</sup>

<sup>1</sup>Institute for Clinical Chemistry and Pathobiochemistry, Department for Diagnostic Laboratory Medicine, University Hospital Tuebingen, Tuebingen, Germany; <sup>2</sup>Key Laboratory of Separation Science for Analytical Chemistry, Dalian Institute of Chemical Physics, Chinese Academy of Sciences, Dalian, China; <sup>3</sup>Research Unit Protein Science, Helmholtz Center Munich, Munich, Germany; <sup>4</sup>Key Laboratory of Tea Biology and Resources Utilization, Ministry of Agriculture, Tea Research Institute, Chinese Academy of Agricultural Sciences, Hangzhou, China; <sup>5</sup>Institute for Diabetes Research and Metabolic Diseases of the Helmholtz Center Munich at the University of Tuebingen, Tuebingen, Germany; <sup>6</sup>German Center for Diabetes Research, Tuebingen, Germany; <sup>7</sup>Leibniz-Institut für Analytische Wissenschaften - ISAS, Dortmund, Germany; <sup>8</sup>Institute of Molecular Toxicology and Pharmacology, Helmholtz Center Munich, German Research Center for Environmental Health GmbH, Neuherberg, Germany; <sup>9</sup>Institute of Toxicology and Environmental Hygiene, Technical University Munich, Munich, Germany; <sup>10</sup>Department of General, Visceral and Transplant Surgery, University Hospital Tuebingen, Tuebingen, Germany; <sup>11</sup>German Cancer Consortium (DKTK) and German Cancer Research Center (DKFZ) Partner Site, Tuebingen, Germany; <sup>12</sup>Medizinisches Proteom-Center, Ruhr-University Bochum, Bochum, Germany; and <sup>13</sup>Department of Chemistry, College of Physical Sciences, University of Aberdeen, Aberdeen, United Kingdom

Submitted 6 March 2019; accepted in final form 12 June 2019

**Kappler L, Hoene M, Hu C, von Toerne C, Li J, Bleher D, Hoffmann C, Böhm A, Kollipara L, Zischka H, Königsrainer A, Häring HU, Peter A, Xu G, Sickmann A, Hauck SM, Weigert C, Lehmann R.** Linking bioenergetic function of mitochondria to tissue-specific molecular fingerprints. *Am J Physiol Endocrinol Metab* 317: E374–E387, 2019. First published June 18, 2019; doi:10.1152/ajpendo.00088.2019.—Mitochondria are dynamic organelles with diverse functions in tissues such as liver and skeletal muscle. To unravel the mitochondrial contribution to tissue-specific physiology, we performed a systematic comparison of the mitochondrial proteome and lipidome of mice and assessed the consequences hereof for respiration. Liver and skeletal muscle mitochondrial protein composition was studied by data-independent ultra-high-performance (UHP)LC-MS/MS-proteomics, and lipid profiles were compared by UHPLC-MS/MS lipidomics. Mitochondrial function was investigated by high-resolution respirometry in samples from mice and humans. Enzymes of pyruvate oxidation as well as several subunits of complex I, III, and ATP synthase were more abundant in muscle mitochondria. Muscle mitochondria were enriched in cardiolipins associated with higher oxidative phosphorylation capacity and flexibility, in particular CL(18:2)<sub>4</sub> and 22:6-containing cardiolipins. In contrast, protein equipment of liver mitochondria indicated a shuttling of complex I substrates toward gluconeogenesis and ketogenesis and a higher preference for electron transfer via the flavoprotein quinone oxidoreductase pathway. Concordantly, muscle and liver mitochondria showed distinct respiratory substrate preferences. Muscle respired significantly more on the complex I substrates pyruvate and glutamate, whereas in liver maximal respiration was supported by complex II substrate succinate. This was a consistent finding in mouse liver and

skeletal muscle mitochondria and human samples. Muscle mitochondria are tailored to produce ATP with a high capacity for complex I-linked substrates. Liver mitochondria are more connected to biosynthetic pathways, preferring fatty acids and succinate for oxidation. The physiologic diversity of mitochondria may help to understand tissue-specific disease pathologies and to develop therapies targeting mitochondrial function.

cardiolipins; liver; mitochondria; multi-omics; muscle

## INTRODUCTION

Mitochondria are in the focus of basic and translational research because of their central metabolic function and their involvement in the pathophysiology of human diseases such as neurodegenerative disorders, cancer, and diabetes (56). Even though it is evident that mitochondria must be well adapted for the different functions of organs in metabolism, only few studies report tissue-specific characteristics, and most of these studies just focus on one aspect such as mitochondrial morphology, protein abundance, or oxidative capacity (3, 20, 25, 35). Mitochondria and their function are often rather generalized among tissues, and mitochondrial (dys)function is examined in disease pathologies without paying attention to probable tissue specificities. We believe that the investigation of the specific mitochondrial characteristics in disease-related tissues might lead to more specific and thus effective understanding and forward-thinking treatments of mitochondria-related diseases.

Two types of molecules are the central executors and regulators of mitochondrial function: proteins and lipids. Since proteins perform almost all relevant metabolic conversions in

Address for reprint requests and other correspondence: R. Lehmann, Institute for Clinical Chemistry and Pathobiochemistry, Dept. of Diagnostic Laboratory Medicine, Univ. Hospital Tuebingen, Hoppe-Seyler-Str.3, 72076 Tuebingen, Germany (e-mail: rainer.lehmann@med.uni-tuebingen.de).

mitochondria, determination of protein abundances in different tissues is the first step to understanding the molecular determinants of the divergent metabolic activities adapted specifically to diverse cellular and tissue requirements. Lipids on the other hand, in addition to being a membrane constituent and energy source, are involved in physiological processes such as mitochondrial fusion and fission, fine tune membrane structure and fluidity, and participate in electron transport chain assemblage, protein biogenesis, apoptosis, and many other processes (6, 17, 36). Taken together, lipids regulate mitochondrial function on many levels, and changes in lipid homeostasis and membrane composition are very likely to regulate both mitochondrial structure and function (14, 17). We started our tissue-specific investigation of mitochondria with skeletal muscle and liver, two insulin target tissues playing a central role in the origin and progression of diabetes. A (dys)function of mitochondria in these tissues is often discussed as central to diabetes development (23, 24, 34, 42).

Skeletal muscle and liver mitochondria have quite distinctly different physiological tasks. Mitochondria in skeletal muscle face large variances in ATP demands upon physical activity, requiring greater variations in the rate of metabolism than any other tissue. Skeletal muscle is responsible for over 80% of postprandial glucose disposal (7) and is furthermore considered to be the major organ for fatty acid disposal because of its relative size in men and most animals (11). Liver on the other hand balances supply and blood concentration of glucose by the release of glucose from glycogenolysis and gluconeogenesis. Liver contributes to a major extent to total glucose production (45), and it is the major site of fatty acid production in humans (39). Intrahepatic fatty acids are used for oxidation, storage, or for packaging them into lipoproteins for export and storage or use in other tissues (43). In states of prolonged exercise or fasting, hepatic mitochondrial ketogenesis provides acetoacetate and 3-hydroxybutyrate as substrates not only for peripheral tissues like the skeletal muscle but also brain and heart (30).

We hypothesize that these major differences in metabolic pathways are reflected by differences in both mitochondrial protein equipment and lipid composition of liver and skeletal muscle with consequences on respiratory function. Therefore, we applied a systemic approach combining proteomics and lipidomics analyses with high-resolution respirometry to understand tissue-specific mitochondrial function and organization. Tissue-specific physiological diversity was revealed in hepatic and skeletal muscle mitochondria from mice and validated in human samples.

## MATERIALS AND METHODS

### Chemicals

Bradford Reagent was from Carl Roth (Karlsruhe, Germany). Infrared fluorescent dye secondary antibodies (anti-mouse/-rabbit/-guinea pig) were purchased from LI-COR (Lincoln, NE). Anti-medium-chain acyl-CoA dehydrogenase (cat. no. sc-365448) and anti-pyruvate dehydrogenase (cat. no. sc377092) were from Santa Cruz Biotechnology (Dallas, TX). Anti-pyruvate carboxylase (cat. no. SAB2500845) was purchased from Sigma-Aldrich (Munich, Germany). Anti-OXPHOS-Cocktail (cat. no. ab110413), anti-citrate synthase (cat. no. ab96600), and anti-ECHA (cat. no. ab54477) antibodies were purchased from Abcam (Cambridge, UK). The anti-COX4 antibody (cat. no. 4844S) was purchased from Cell Signaling Tech-

nology (Danvers, MA). MS or LC grade solvents acetonitrile (ACN), methanol, and isopropanol were purchased from Merck (Darmstadt, Germany). Ammonium acetate was purchased from Sigma-Aldrich. Ultrapure water was prepared by a Milli-Q system (Millipore). The synthetic lipid standards d4-palmitic acid, CER(d18:1/17:0), LPC(19:0), PC(19:0)<sub>2</sub>, PE(15:0)<sub>2</sub>, SM(d18:1/12:0), TG(15:0)<sub>3</sub>, CL(14:0)<sub>4</sub>, CL(14:1)(24:1)<sub>3</sub>, CL(14:1)<sub>3</sub>(15:1), CL(15:0)<sub>3</sub>(16:1), and CL(14:1)(22:1)<sub>3</sub> were purchased from Avanti Polar Lipids (Alabaster, AL) or Sigma-Aldrich. High-resolution respirometry substrates and inhibitors antimycin A, carbonylcyanide p-trifluoromethoxyphenylhydrazone (FCCP), cytochrome c, malate, pyruvate, rotenone, and succinate were purchased from Sigma-Aldrich. Adenosine diphosphate was purchased from Calbiochem, Merck, and octanoylcarnitine from Tocris Bioscience (Bristol, UK).

### Methods

**Animal care.** The animal experiment was performed in accordance with the Directive 2010/63/EU of the European Union and the German Animal Welfare Act and approved by the local authorities (Regierungspraesidium Tuebingen). Investigations were performed in tissues of 18-wk-old male C57Bl/6N mice. Mice were purchased from Charles River (Sulzfeld, Germany) at an age of 9 wk and fed a purified standard diet (E157453-04, Ssniff, Soest, Germany) ad libitum. For organ harvesting, mice were anaesthetized with an intraperitoneal injection of ketamine and xylazine (150 and 10 mg/kg body wt, respectively) and exsanguinated by decapitation.

**Human samples.** Skeletal muscle biopsies were obtained by percutaneous needle biopsies performed on the vastus lateralis of the quadriceps femoris after local anesthesia (2% Scandicaine; Aspen Pharma GmbH, Munich, Germany) from untrained participants (6 females, 2 males) before an exercise training intervention study. Informed written consent was given by all individuals; the study protocol was approved by the ethics committee of the University of Tuebingen (446/2016BO2) and was in accordance with the Declaration of Helsinki. The fresh human liver tissue was collected during hepatic surgery that was performed for different reasons, e.g., hepatic hemangioma, curative resection of hepatic metastases of colorectal malignancies, or hepatocellular carcinoma, at the Department of General, Visceral, and Transplant Surgery at the University Hospital of Tuebingen. Only samples from normal, nondiseased tissue judged by an experienced pathologist were used. Patients fasted overnight before collection of liver samples (2 females, 1 male). Exclusion criteria were viral hepatitis infection and liver cirrhosis. Informed, written consent was obtained from all participants, and the ethics committee of the University of Tuebingen approved the protocol (239/2013BO1) that was in accordance with the Declaration of Helsinki.

**Mitochondria isolation.** Mitochondria isolation was performed as previously described (22) with some modifications. A scheme of the experimental workflow is given in Supplemental Fig. SA1 (Supplemental Material A is available at <https://doi.org/10.6084/m9.figshare.7993946.v1>). All isolation steps were performed at 4°C or on ice. The homogenization procedure was different for each tissue: 150 mg liver were directly placed into ice-cold sucrose-Tris-EGTA (STE) buffer (250 mM sucrose, 5 mM Tris, 2 mM EGTA, 0.5% BSA, pH 7.4 at 4°C). Tissue was cut into small pieces, homogenized using a loosely fitted 2-mL glass-glass Dounce (Sartorius, Goettingen, Germany) by applying 6 strokes, transferred to a 50-mL tube, and filled up with STE + 0.5% BSA. For the homogenization of muscle, 550 mg pooled upper hind limb skeletal muscle tissue (mostly type 2 fibers) was directly transferred into ice-cold PBS (Sigma-Aldrich). Tissue was cut into small pieces, transferred to a 50-mL tube, and digested for 3 min at 4°C with type VIII protease from *Bacillus licheniformis* (Sigma-Aldrich). One milliliter of enzyme solution [6 mg protease (10 U/mg)/mL STE] was added to 100 mg tissue. After 3 min, 10 mL STE + 0.1% BSA was added, and the sample was

centrifuged for 30 s at 900 g at 4°C. Supernatant was removed, the tube filled up with STE + 0.1% BSA, and centrifuged again. This washing step was repeated three times in total. The muscle suspension was then homogenized using a 15-mL Teflon-glass Dounce (Sartorius, Goettingen, Germany). After the tissue-specific homogenization procedure, all following centrifugation steps and procedures were similar for both homogenates. The homogenates were centrifuged at 900 g for 10 min. The supernatant was transferred into a new centrifuge tube and centrifugation was repeated. The supernatant was then centrifuged at 9,000 g for 10 min to pellet the crude mitochondrial fraction. The pellet was resuspended in STE + 0.1% BSA and centrifuged again at 9,000 g for 10 min. The crude mitochondrial pellet was carefully resuspended in 200  $\mu$ L STE. An aliquot was used to determine the total protein concentration using Bradford reagent. One hundred micrograms of this mitochondrial suspension was used for respiration analyses as described below. The remaining mitochondrial suspension was layered on 5-mL Percoll gradient (25%) and centrifuged for 20 min at 80,000 g. The lower of the 2 appearing layers was collected with a Pasteur pipette and transferred to a new centrifuge tube, filled up with STE without BSA, and centrifuged 10 min at 9,000 g. The pellet was resuspended in a small volume of STE buffer without BSA. After centrifugation at 16,000 g for 2 min, the supernatant was removed, the pellet was resuspended in PBS, and protein concentration was determined using bicinchoninic acid assay (Pierce BCA Protein Assay Kit, Rockford, IL). Aliquots with specific protein amounts for lipidomics, Western blotting, and proteomics were frozen at  $-80^{\circ}\text{C}$ .

**Tissue lysis, electrophoresis, and Western blot analysis.** For whole tissue Western blot analysis, mouse liver and skeletal muscle tissue were homogenized in cold 1 mL radioimmunoprecipitation assay lysis buffer (25 mM Tris, 150 mM NaCl, 0.1% SDS, 0.5% NaDOC, 1% Triton-X-100; pH 7.6) using a TissueLyser (Qiagen, Hilden, Germany). The settings were 2 min at 20 Hz for liver and 4 min at 20 Hz for muscle tissue. The lysate was centrifuged for 10 min at 13,000 g at 4°C. Supernatant was transferred to a new cup, and centrifugation was repeated. The supernatant from the second centrifugation was aliquoted and stored at  $-80^{\circ}\text{C}$ . Immunoblots from 30  $\mu$ g protein from tissue lysate or isolated mitochondrial fraction were performed as described (22) using IRDye secondary antibodies (LI-COR Biosciences GmbH, Bad Homburg, Germany).

**Proteomic sample preparation.** Ten micrograms of sample was subjected to tryptic digest using a modified filter-aided sample preparation protocol (13, 57) with the following changes: a buffer was added to each sample containing urea and SDS in a final concentration of 4 M and 2%, respectively. Samples were reduced at room temperature. Peptides were stored at  $-80^{\circ}\text{C}$  until MS measurement.

**Ultra-high-performance LC-MS/MS-proteomics.** Label-free LC-MS/MS-based proteomics measurements were performed using data-independent acquisition (DIA), which allows for the identification of a broad range of proteins along with a reproducible relative quantification (18, 47). MS data were acquired on a Q Exactive high-field mass spectrometer (Thermo Fisher Scientific, Rockford, IL). Approximately 0.5  $\mu$ g per sample spiked with 1 injection unit of the hyper reaction monitoring (HRM) Calibration Kit (Biognosys, Schlieren, Switzerland, cat. no. K-3003) for retention time indexing were automatically loaded to the online coupled ultra-high-performance liquid chromatography (UHPLC) system (Ultimate 3000, Thermo Fisher Scientific). A nano trap column was used (300- $\mu$ m inner diameter  $\times$  5 mm, packed with Acclaim PepMap100 C18, 5  $\mu$ m, 100  $\text{\AA}$ ; LC Packings, Sunnyvale, CA) before separation by reversed phase chromatography (Acquity UHPLC M-Class HSS T3 Column 75  $\mu$ m ID  $\times$  250 mm, 1.8  $\mu$ m; Waters, Eschborn, Germany) at 40°C. Peptides were eluted from the column at 250 nL/min using increasing ACN concentration (in 0.1% formic acid) from 3% to 41% over a 105-min gradient. The DIA method consisted of a survey scan from 300 to 1,650 mass-to-charge ratio at 120,000 resolution and an automatic gain control (AGC) target of 3e6 or 120 ms maximum injection time.

Fragmentation was performed via higher energy collisional dissociation with a target value of 3e6 ions determined with predictive AGC. Precursor peptides were isolated with 37 variable windows spanning from 300 to 1,650 mass-to-charge ratio at 30,000 resolution with an AGC target of 3e6 and automatic injection time. The normalized collision energy was 28, and the spectra were recorded in profile mode.

For label-free quantification of DIA data, the DIA LC-MS/MS data set was analyzed by comparing the MS2 fragment spectra from the recorded windows (see above) against a spectral library collected from data-dependent acquisition data (164 raw files) from the same instruments. These data-dependent acquisition raw files were analyzed by using Proteome Discoverer (version 2.1, Thermo Fisher Scientific) and applying a Byonic (version 2.0, Proteinmetrics, San Carlos, CA) search engine node maintaining 1% peptide and protein false discovery rate (FDR) threshold. Results were merged into a spectral library using Spectronaut (Version 10, Biognosys, Schlieren, Switzerland) with default settings using the Proteome Discoverer result file. Spectronaut was equipped with the Swissprot mouse database (release 2017.02, 16,869 sequences, <https://www.uniprot.org/>) with a few spiked proteins (e.g., Biognosys HRM peptide sequences). The final spectral library generated in Spectronaut contained 10,525 protein groups and 322,041 peptide precursors.

Quantification was based on cumulative MS2 area levels. Briefly, a Spectronaut HTRMS converter was used to convert the raw files with the data, and XIC extraction settings were set to dynamic with a correction factor of one. Automatic calibration mode was chosen with nonlinear retention time recalibration based on the spiked HRM peptides enabled. Interference correction on MS1 and MS2 level was enabled. Peptide identification was filtered to satisfy an FDR of 1% by the mProphet approach (44). Only proteotypic peptides were considered for protein quantification applying summed precursor quantities based on MS2 area quantity. A match between runs was enabled with the q-value percentile mode 0.25 threshold. This setting filters for proteins that fulfill the 1% FDR threshold in at least 25% of all samples.

Abundances of individual proteins were expressed as percentages of total protein abundance in a given sample to compensate for overall differences in protein abundance between samples. To estimate the purity of the mitochondrial fractions, proteomics data were queried against the Mitominer database [Mitominer 4.0 (51)]; the query was performed based on gene symbols.

**Sample preparation for lipidomics.** Lipids were extracted with methyl tert-butyl ether as described previously (5). Briefly, water was added to 50  $\mu$ g (by protein) of mitochondrial suspension to reach a total volume of 100  $\mu$ L. Next, 350  $\mu$ L of ice-cold methanol including internal standards was added. Samples were briefly vortexed, 1 mL of methyl tert-butyl ether was added, and the samples were shaken for 30 min at room temperature. After adding 250  $\mu$ L of water and incubating the sample at room temperature for 10 min, samples were centrifuged for 20 min at 1,000 g and 4°C to induce phase separation.

**UHPLC-MS/MS-lipidomics.** Lipidomics profiling was performed in a Waters UHPLC system (Milford, MA) coupled with a Q Exactive high-field mass spectrometer (Thermo Fisher Scientific). Separation of lipid metabolites was achieved in a Waters UHPLC C8 ACQUITY column (100 mm  $\times$  2.1 mm  $\times$  1.7  $\mu$ m). The elution solvents consisted of A (ACN:H<sub>2</sub>O = 60:40, vol/vol) and B (isopropanol:ACN = 90:10, vol/vol), both containing 10 mM ammonium acetate. The elution gradient started at 32% B for the initial 1.5 min, followed by a linear increase to 85% B during the next 14 min. Within the subsequent 0.1 min, solvent B was rapidly increased to 97% and then maintained for 2.4 min for column flush. Subsequently, the elution solvent was returned to 32% B within 0.1 min and kept for 1.9 min for column equilibration. The column temperature was set to 55°C, and the flow rate was 0.26 mL/min. Lipidomics data were acquired in both electrospray ionization-positive and -negative modes at scan ranges of 400–1,300 Da and 200–1,800 Da, respectively. The spray voltage

was 3.5 kV for positive mode and  $-3.0$  kV for negative mode. The capillary temperature was maintained at  $300^{\circ}\text{C}$ . The auxiliary gas heater temperature was set to  $350^{\circ}\text{C}$ . The flow rate of sheath gas and auxiliary gas was 45 arbitrary units and 10 arbitrary units, respectively. The S-lens RF level was 50. The AGC target was set to be  $3 \times 10^6$  ion capacity, and maximum IT was 200 ms. Mass resolution was 120,000 and 30,000 for full scan MS and data-dependent MS/MS. Lipid identities were assigned based on accurate mass measurement, MS/MS fragmentation, and LC elution behavior. Ninety-five percent of all detected lipids showed a relative standard deviation below twenty percent throughout nine injections of a pooled sample during the whole UHPLC-MS run. All detected lipids were quantified by normalization to the corresponding internal standard.

**Functional assay.** Mitochondrial function was investigated by respiration measurements in an Oxygraph-2k (Oroboros Instruments, Innsbruck, Austria). Crude mitochondrial suspension ( $100 \mu\text{g}$ ) was placed in Mir05 buffer [ $0.5 \text{ mM EGTA}$ ,  $3 \text{ mM MgCl}_2(\text{H}_2\text{O})_6$ ,  $60 \text{ mM K-lactobionate}$ ,  $20 \text{ mM taurine}$ ,  $10 \text{ mM KH}_2\text{PO}_4$ ,  $20 \text{ mM HEPES}$ ,  $110 \text{ mM sucrose}$ ,  $1 \text{ g/L BSA}$ ,  $\text{pH} = 7.1$  at  $30^{\circ}\text{C}$ ] in the Oxygraph-2k chambers. Malate ( $1.28 \text{ mM}$ ),  $0.5 \text{ mM}$  octanoylcarnitine (fatty acid oxidation),  $2.5 \text{ mM ADP}$  (phosphorylating condition),  $5 \text{ mM pyruvate}$  or  $10 \text{ mM glutamate}$  (complex I respiration),  $2.5 \text{ mM succinate}$  (complex II respiration),  $10 \mu\text{M}$  cytochrome c (integrity control), FCCP in  $0.5 \mu\text{M}$  steps (uncoupled state),  $1.25 \mu\text{M}$  rotenone (complex I inhibitor), and  $5 \mu\text{M}$  antimycin A (complex III inhibitor) were added to evaluate electron transport chain capacity and nonmitochondrial oxygen consumption. Cytochrome c effect as control for integrity was  $18.1 \pm 3.6\%$  for liver mitochondria and  $4.8 \pm 2.3\%$  for muscle mitochondria. Liver and muscle mitochondria were isolated from tissues of the same animal. Further experiments were  $1.28 \text{ mM malate}$ ,  $5 \text{ mM pyruvate}$  or  $10 \text{ mM glutamate}$ ,  $2.5 \text{ mM ADP}$ ,  $0.5 \text{ mM octanoylcarnitine}$ ,  $10 \mu\text{M}$  cytochrome c (integrity control), FCCP in  $0.5 \mu\text{M}$  steps (uncoupled state),  $1.25 \mu\text{M}$  rotenone (complex I inhibitor), and  $5 \mu\text{M}$  antimycin A (complex III inhibitor). Data were corrected for nonmitochondrial background by subtraction of antimycin A oxygen consumption.

**Respiratory measurements of human samples.** Muscle fibers were skinned as previously published by Pesta and Gnaiger (40) with modifications. Muscle biopsies were directly placed in the Mir05 buffer. During skinning of the fibers in a 6-well plate, the dissected fibers were placed in a  $70\text{-}\mu\text{m}$  cell strainer (BD Falcon, Franklin Lakes, NJ). After skinning, the fibers were washed three times instead of only once, and the measurement in the Oxygraph-2k was performed under normal air oxygen pressure without the usage of catalase and  $\text{H}_2\text{O}_2$ . Two milligrams of muscle fibers was used for respiratory analysis. Two milligrams of liver was weighed and cut into small pieces before being placed in the Oxygraph-2k, and digitonin was added to permeabilise the tissue. Measurements were performed as described above for mouse mitochondria. Cytochrome c effect was  $4.4 \pm 1.9\%$  for liver and  $5.9 \pm 5.1\%$  for muscle fibers.

**Statistical analysis.** Proteomics, lipidomics, and high-resolution respirometry were performed with isolated mitochondria from 8 mice ( $n = 8$ ; because of logistical reasons respirometry was only measured with  $n = 5$  for isolated liver mitochondria). Follow-up respirometry for further characterization of the substrate preference was performed with another set of 5 mice ( $n = 5$  for liver and muscle mitochondria). For functional and Western blot analyses, statistical significance was evaluated by a Student's *t*-test using GraphPad Prism (GraphPad Software, La Jolla, CA).  $P < 0.05$  was considered significant. The open-source MultiExperiment Viewer software (46) was employed for heatmap generation using mean-centered data prescaled to unit variance. Multivariate principal component analysis was performed on the lipid concentrations per microgram mitochondrial protein with SIMCA-P 11.5 (Umetrics, Umeå, Sweden). Data were unit variance scaled and log transformed using the auto transformation option. The content of individual phosphatidylglycerols (PGs) and lipid cardiolipins (CLs) was divided by the sum of all PGs and CLs, respectively,

to calculate the percent contribution of individual species. The sum of acyl chains within CLs was obtained by multiplying the content of individual CLs with the number of acyl chains within this CL [e.g.,  $1 \times (18:1)$  and  $3 \times (18:2)$  for  $\text{CL}(18:1)(18:2)_3$ ] and also expressed as percentage. For the statistical analysis of lipidomics and proteomics data, JMP 13.0 (SAS, Cary, NC) was used, considering an FDR  $P$  value  $< 0.05$  as significant.

## RESULTS

**Mitochondria show tissue-specific protein compositions.** First, we analyzed liver and skeletal muscle mitochondrial protein composition by data-independent proteomics to elucidate the molecular basis for tissue-specific differences. Mitochondria were isolated from mouse liver and upper hind limb muscles consisting mainly of type 2 fibers. Proteins with known mitochondrial localization according to the Mitominer 4.0 database (51) accounted for 89% and 86% of total detected protein abundance in liver and muscle mitochondria, respectively. The analysis revealed a quite distinct tissue-specific mitochondrial protein pattern (Fig. 1). In accordance with organ function, muscle mitochondria contained a higher percentage of proteins related to oxidative phosphorylation, ATP synthesis, and pyruvate decarboxylation (Fig. 1, A and B). Two ATP synthase subunits (ATPA, ATPB) and ADP/ATP translocase 1 accounted for 17% of total protein intensity in muscle mitochondria (Fig. 1D). Enzymes of the citric acid cycle were also more abundant in muscle mitochondria. The percentage of proteins related to  $\beta$ -oxidation, in contrast, was higher in liver than in muscle (Fig. 1, A and B). Mitochondrial 3-ketoacyl-CoA thiolase, which catalyzes the last step of  $\beta$ -oxidation, was the second most abundant protein in liver mitochondria (Fig. 1C). Proteins involved in ketogenesis, gluconeogenesis, and amino acid metabolism were also higher in liver mitochondria (Fig. 1, A and B).

The mitochondrial abundance of several subunits of the respiratory chain was different between the tissues (Fig. 2). Almost all subunits of complex I and several of III and V, but also some subunits of complex IV, were more abundant in skeletal muscle than in liver mitochondria (Fig. 2). For complex II, succinate dehydrogenase (SDH) B and SDHC (C560) were higher in muscle mitochondria, whereas SDHA was higher in liver. The electron transfer flavoproteins ETFA, ETFB, and ETFD, which mediate the reduction of ubiquinone by  $\text{FADH}_2$  derived from  $\beta$ -oxidation and amino acid degradation, were also more abundant in liver than in muscle mitochondria.

We also had a closer look on the abundance of mitochondrial proteins determining the route of pyruvate or acetyl-CoA toward mitochondrial oxidation or biosynthetic pathways (Fig. 3). Proteomics analyses revealed higher abundance of the proteins of the pyruvate dehydrogenase complex in muscle. Citrate synthase was also higher in muscle than in liver mitochondria. In contrast, pyruvate carboxylase was highly abundant in liver mitochondria, which links pyruvate to gluconeogenesis. Mitochondrial tricarboxylate transport protein, which exports citrate for cytosolic acetyl-CoA production, was highly abundant in liver mitochondria. This is well in line with the high rate of fatty acid synthesis and ketogenesis in the liver. As shown in Fig. 1, most enzymes of the tricarboxylic acid (TCA) cycle were more abundant in muscle mitochondria, whereas several enzymes involved in  $\beta$ -oxidation were more

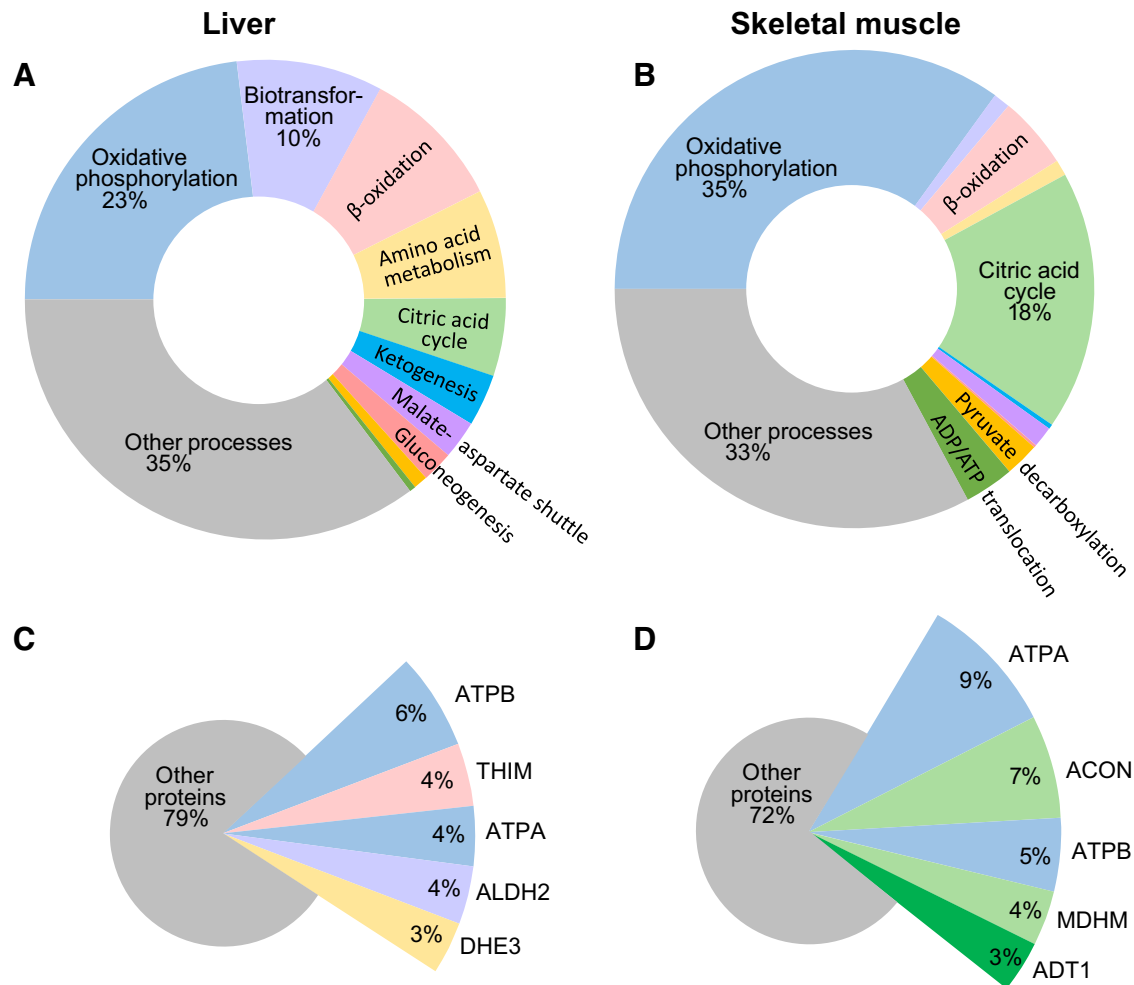


Fig. 1. Composition of mitochondrial proteome from mouse liver and skeletal muscle investigated by LC-MS/MS. Relative contribution of different mitochondrial processes to the total protein intensity in isolated liver (A) and skeletal muscle mitochondria (B). Contribution of the five most abundant proteins to the total detected protein intensity in isolated liver (C) and skeletal muscle (D) mitochondria ( $n = 8$ ). Colors in C and D correspond to A and B. ACON, aconitate hydratase; ADT1, ADP/ATP translocase 1; ALDH2, aldehyde dehydrogenase; ATPA, ATP synthase subunit alpha; ATPB, ATP synthase subunit beta; DHE3, glutamate dehydrogenase 1; MDHM, mitochondrial malate dehydrogenase; THIM, mitochondrial 3-ketoacyl-CoA thiolase. For details of the proteomics data, see Supplemental Material B (available online at <https://doi.org/10.6084/m9.figshare.7993766.v1>).

abundant in liver mitochondria. Of note, in addition to SDHA, succinate-CoA ligase showed higher abundance in liver mitochondria (Fig. 3).

Comparison of the results obtained by proteomics with Western blot analysis revealed a reasonable overlap indicating a good suitability of the widely used antibodies to capture differences in mitochondrial protein abundance. The data showed higher abundance of citrate synthase and of four out of five electron transport chain complexes in isolated muscle compared with liver mitochondria (Fig. 4). The difference in complex III did not reach statistical significance (Fig. 4E). We also investigated the abundance of some of these proteins in total tissue lysates by Western blot analyses (Fig. 5A). Similar to isolated mitochondria, citrate synthase and pyruvate dehydrogenase were higher in skeletal muscle, whereas pyruvate carboxylase was pronouncedly higher in the liver (Fig. 5, B–D). Western blot analysis of medium-chain acyl-CoA dehydrogenase and ECHA confirmed the higher abundance of enzymes of  $\beta$ -oxidation in liver tissue compared with skeletal muscle tissue (Fig. 5, E and F).

*Mitochondria from skeletal muscle show higher phospholipid levels than from liver.* Next, the lipid profile of the isolated mouse liver and skeletal muscle mitochondria was investigated by UHPLC-MS/MS analyses. The tissue origin had no major effect on the total number of detected lipid species (Supplemental Fig. SA1), but tissue differences in the lipid profiles were obvious, as shown by multivariate principal component analysis (Supplemental Fig. SA2). In the direction of the first principal component, a pronounced separation of the clustered hepatic and skeletal muscle-derived mitochondrial samples could be seen. Muscle mitochondria had a higher total lipid content than liver mitochondria ( $316 \pm 49$  pmol lipids/ $\mu$ g total mitochondrial protein vs.  $221 \pm 39$  pmol/ $\mu$ g). Accordingly, most lipid classes were more abundant in muscle mitochondria (Table 1).

To assess differences in membrane lipid composition of liver and muscle mitochondria, data were normalized to total phospho- and sphingolipid content, which was  $262 \pm 41$  pmol/ $\mu$ g mitochondrial protein in muscle mitochondria and  $173 \pm 35$  pmol/ $\mu$ g mitochondrial protein in liver mito-

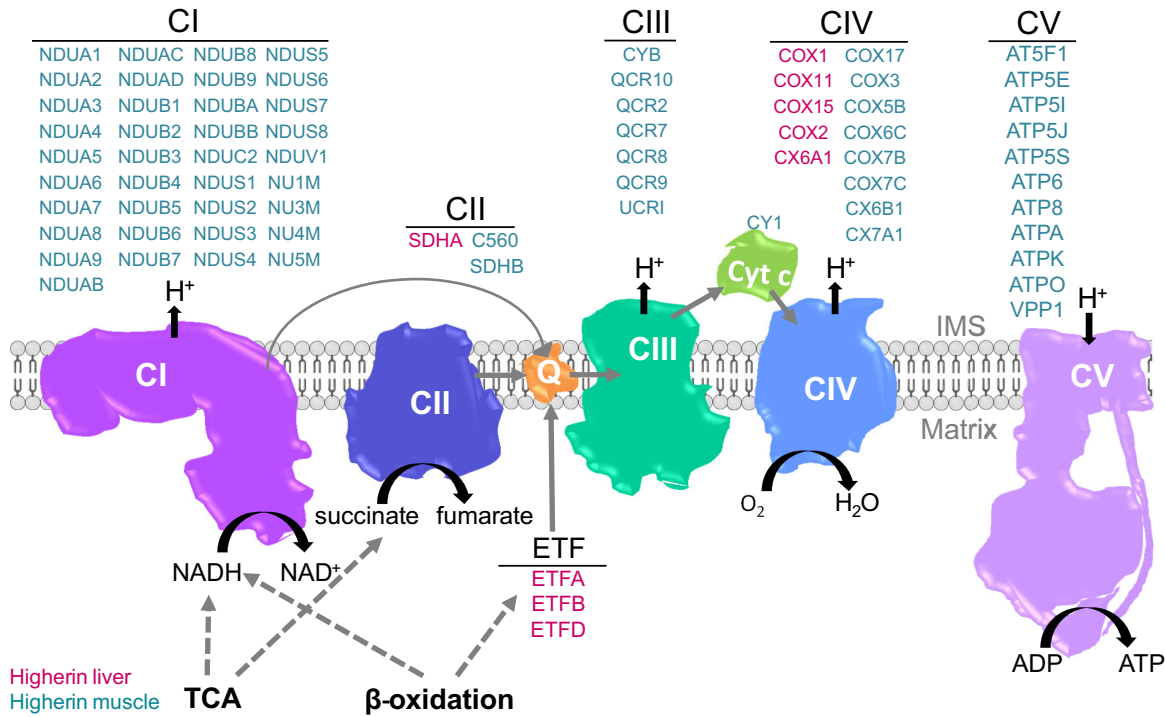


Fig. 2. Proteins of the respiratory chain complexes with different relative abundance in the mitochondrial proteome of mouse liver and skeletal muscle investigated by LC-MS/MS. Solely significantly different proteins are shown. Colors represent higher abundance of proteins in muscle (blue) and liver (red) mitochondria ( $n = 8$ ). The Response Screening platform in JMP 13.0 (SAS, Cary, NC) was used, considering a false discovery rate  $P$  value  $< 0.05$  as significant. CI-CIV, complex I to IV; CV, ATP synthase; Cyt c, cytochrome c; ETF, electron transfer flavoprotein; Q, coenzyme  $Q_{10}$  (ubiquinone); SDH, succinate dehydrogenase; TCA, tricarboxylic acid TCA = tricarboxylic acid cycle. For details of the proteomics data, see Supplemental Material B (available online at <https://doi.org/10.6084/m9.figshare.7993766.v1>).

chondria (Table 1). In skeletal muscle, the relative amounts of the mitochondria signature CL and of the CL precursor PG were significantly higher than in liver, as were (lyso) phosphatidylethanolamines (PEs), lysophosphatidylcholines, and

phosphatidylserines (Table 2). Relative amounts of ceramides, (lyso)phosphatidylinositols, and phosphatidylcholines were significantly higher in liver than in muscle mitochondria (Table 2). The contribution of sphingomyelin to membrane lipid

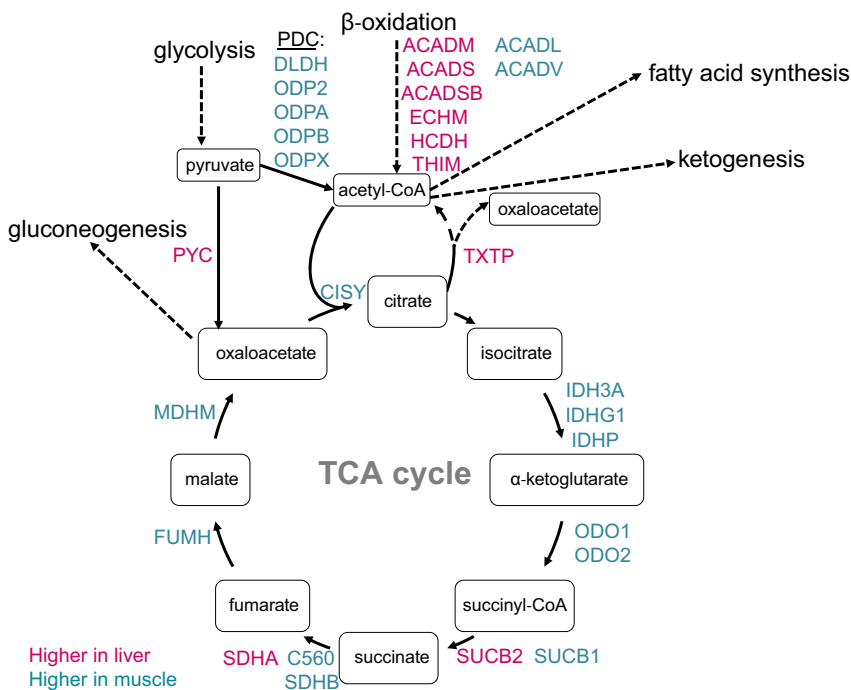


Fig. 3. Proteins of pyruvate and fatty acid oxidation with different relative abundance in the mitochondrial proteome of mouse liver and skeletal muscle investigated by LC-MS/MS. Solely significantly different proteins are shown. Colors represent higher abundance of proteins in muscle (blue) and liver mitochondria (red) ( $n = 8$ ). The Response Screening platform in JMP 13.0 (SAS, Cary, NC) was used, considering a false discovery rate  $P$  value  $< 0.05$  as significant. ACADM, medium-chain acyl-CoA dehydrogenase; CYSY, citrate synthase; ECHM, enoyl-CoA hydratase; FUMH, fumarate hydratase; IDH, isocitrate dehydrogenase; MDHM, mitochondrial malate dehydrogenase; ODO, 2-oxoglutarate dehydrogenase; ODP, pyruvate dehydrogenase; PDC, pyruvate dehydrogenase complex; PYC, pyruvate carboxylase; SDH, succinate dehydrogenase; SUCB2, succinate-CoA ligase; TCA, tricarboxylic acid; THIM, mitochondrial 3-ketoacyl-CoA thiolase. For details of the proteomics data, see Supplemental Material B (available online at <https://doi.org/10.6084/m9.figshare.7993766.v1>).

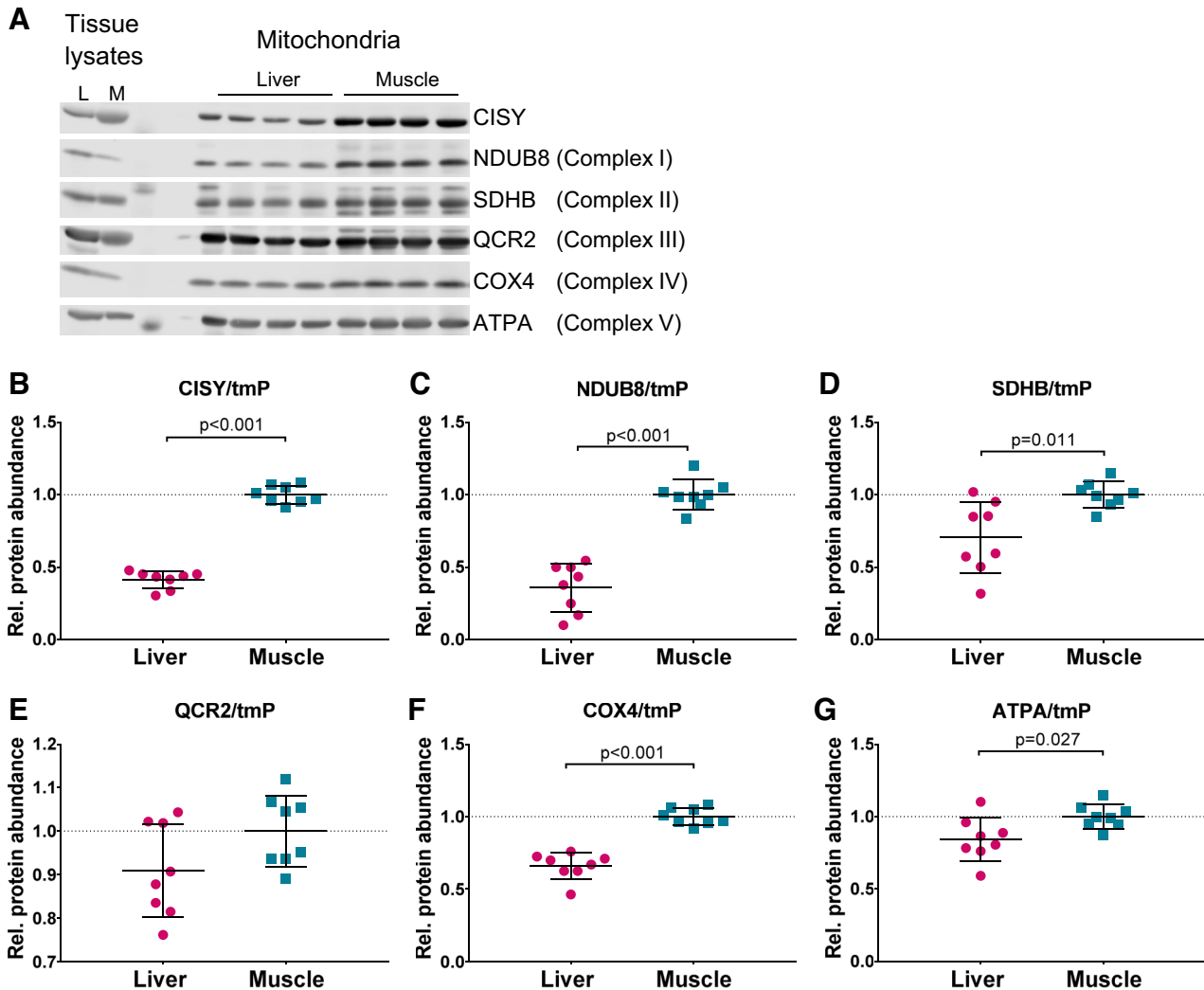


Fig. 4. Analysis of electron transport chain complexes in purified mitochondria of mouse liver and skeletal muscle. Representative Western blot (A) of 4 mitochondria isolations per tissue and densitometric quantification. Equal protein amounts ( $30 \mu\text{g}$ ) of total cell lysates and mitochondria were loaded on the same blot to determine the protein levels before mitochondrial enrichment. Mitochondrial citrate synthase (CISO) was assessed as common mitochondrial marker protein (B). For the detection of the electron transport chain complexes (C–G), an antibody cocktail was used against NDUB8 (complex I), succinate dehydrogenase (SDHB) (complex II), QCR2 (complex III), and ATP synthase subunit alpha (ATPA) (complex V). A separate antibody was used for complex IV (COX4; F). Signals were normalized to total protein abundance determined via stain-free 2,2,2-trichloroethanol. Histograms (B–G) show the densitometric quantifications of Western blots ( $n = 8$ , mean of “muscle” set to 1). Data are presented as means  $\pm$  SD. Statistical significance was evaluated by Student’s *t*-test. NDUB8, NADH dehydrogenase [ubiquinone] 1 beta subcomplex subunit 8; QCR2, cytochrome b-c1 complex subunit 2; rel, relative; tmP, total mitochondrial protein.

content of mitochondria derived from liver or muscle was equal (Table 2).

*Cardiolipins have a different acyl chain composition in mouse muscle and liver mitochondria.* CLs are the only mitochondria-specific lipids. To compare the patterns of CLs and of their precursor lipids PGs, levels of individual species were normalized to the sum of CL (Fig. 6). The most abundant CL species in muscle contained four 18:2 acyl chains ( $25.5 \pm 4.3\%$  in muscle vs.  $13.6 \pm 3.2\%$  in liver mitochondria). In both tissues, 18:2 was the most abundant acyl chain present in CL ( $55.2\%$  of all acyl chains in muscle vs.  $47.3\%$  in liver mitochondria, Table 3). A striking finding was the higher amount of 22:6 acyl chains in CLs of skeletal muscle mitochondria compared with liver; 22:6 was found in 4 of the 24 CL species and accounted for 4.6% of all CL acyl chains in muscle and 1.7% in liver (Table 3). Interestingly, PGs containing 22:6 acyl chains were

significantly lower or below the detection limit in muscle, possibly indicating a preferential channeling of these acyl chains into CLs (Fig. 6). CLs containing 20:4 acyl chains were more abundant in liver compared with muscle mitochondria.

*Differences in protein composition between liver and skeletal muscle are linked to tissue specificity of mitochondrial function and respiratory substrate preferences.* To elucidate the impact of these differing protein and lipid fingerprints on respiration, we analyzed mouse liver and skeletal muscle mitochondria by high-resolution respirometry. Distinct differences were observed analyzing the complex I- and complex II-linked substrates pyruvate and succinate (Fig. 7, A and B). Muscle mitochondria respired significantly more after the addition of pyruvate, whereas no increase in respiration of liver mitochondria was detectable. This is consistent with the higher abundance of the proteins of the pyruvate dehydrogenase

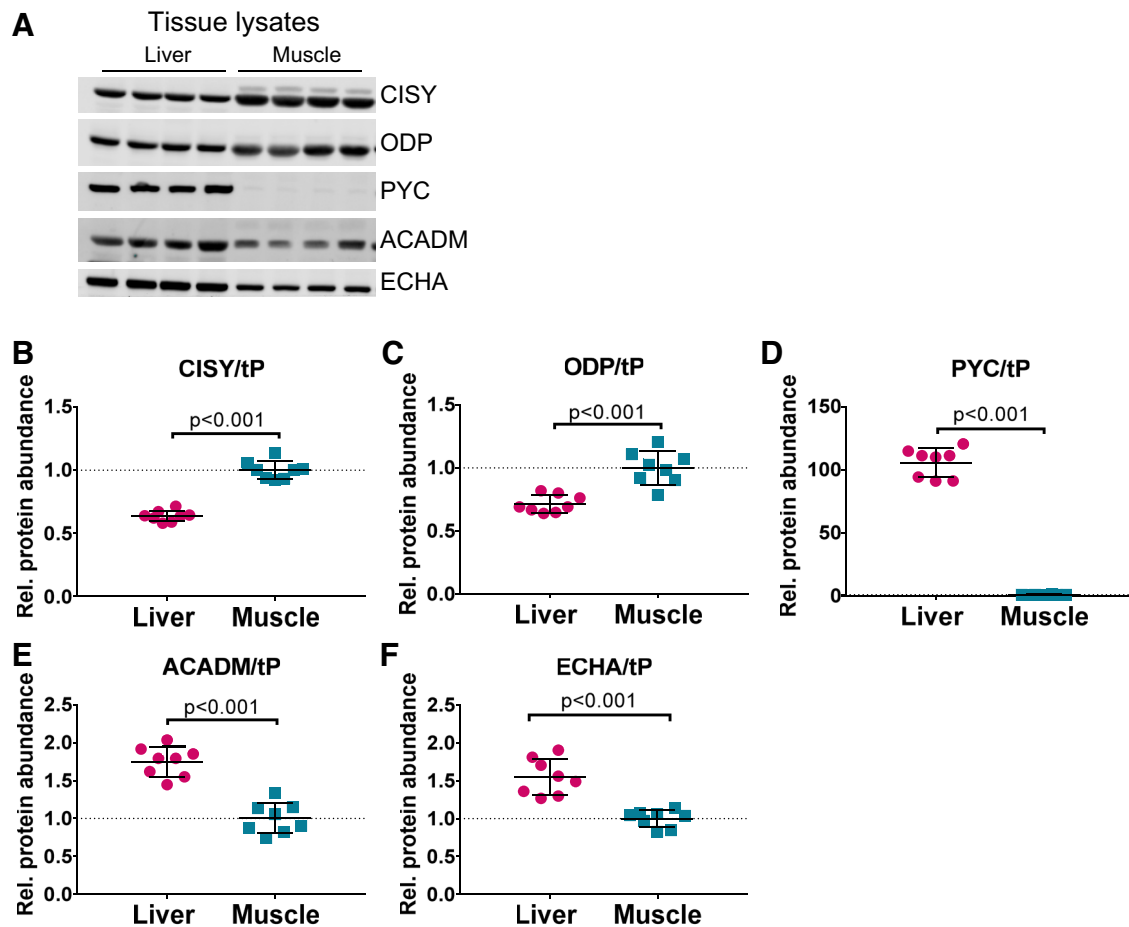


Fig. 5. Quantity of individual proteins related to energy metabolism in tissue lysates of mouse liver and skeletal muscle analyzed by Western blot (A) and densitometric quantification (B–F). A representative Western blot with 4 out of 8 tissue lysates is shown. Mitochondrial citrate synthase (CISY) was used as a mitochondrial marker (B). ODP (C) and PYC (D) were assessed to investigate pyruvate metabolism. ACADM and ECHA were used to assess  $\beta$ -oxidation (E and F). Histograms (B–F) show the sums of the densitometric quantifications of Western blots (mean of “muscle” was set to 1,  $n = 8$ ). Signals are normalized to total protein abundance. Data are presented as means  $\pm$  SD. Statistical significance was evaluated by a Student’s *t*-test. ACADM, medium-chain acyl-CoA dehydrogenase; ECHA, hydroxyacyl-CoA dehydrogenase/3-ketoacyl-CoA thiolase/enoyl-CoA hydratase (trifunctional protein) alpha subunit; ODP, pyruvate dehydrogenase; PYC, pyruvate carboxylase; rel, relative; tP, total protein.

complex in muscle revealed by proteomic analyses, which links the glycolytic pathway to the TCA cycle and by that provides NADH for complex I. In contrast, liver mitochondria respired significantly more after adding the complex II-associated substrate succinate. Accordingly, the contribution of complex II-associated substrate oxidation to maximal respiration on complex I and II substrates was higher in liver as evident after the addition of the complex I inhibitor rotenone. Using glutamate as a complex I-linked substrate instead of pyruvate revealed the same differences between liver and muscle mitochondria (Fig. 7, C–E). To avoid any effects of the combination with the  $\beta$ -oxidation substrate octanoylcarnitine, pyruvate-driven respiration was also studied before adding octanoylcarnitine (Fig. 7, F and G). Again, muscle mitochondria proved to be more prone to the provided complex I-linked substrate pyruvate than liver, and comparable results were obtained with glutamate (Fig. 7H). The subsequent addition of octanoylcarnitine led only in liver mitochondria to a further increase in respiration, independent of the complex I substrate used (Fig. 7I).

It must be taken into account that the mouse skeletal muscle mitochondria were isolated from the upper hind limbs, repre-

sented mostly fast type 2 fibers (4). However, the observed differences in complex I- and II-linked substrate respiration were confirmed in human skeletal muscle fibers isolated from vastus lateralis muscle, which represent a mix of slow type I and fast type 2 fibers (Fig. 7, J–L; Supplemental Fig. SA3) (49). Human muscle fibers showed higher respiration on complex I substrate pyruvate, whereas human liver homogenate showed higher respiration on complex II substrate succinate. These data underline that the different contribution of complex I and II to maximal respiration in liver and muscle mitochondria is of relevance in mice and humans and not restricted to fast muscle fibers.

## DISCUSSION

Here we report a multi-omics approach to provide an overall mitochondrial molecular fingerprint on the levels of lipids and proteins for mouse muscle and liver tissue and additionally link it to respiratory function. Our work indicates a tissue-specific mitochondrial respiratory profile with distinctly different respiratory complex I and II substrate preferences of mitochondria from liver compared with skeletal muscle. Muscle mitochon-



Table 1. Absolute lipid class levels in isolated mitochondria per  $\mu\text{g}$  mitochondrial protein from mouse liver and skeletal muscle

Lipid Class	Mean Liver, pmol/ $\mu\text{g}$	SD Liver	Mean Muscle, pmol/ $\mu\text{g}$	SD Muscle	FDR <i>P</i> Value Muscle vs. Liver
CER	0.79	0.05	0.85	0.07	0.090
CL	12.03	3.07	31.21	6.32	<0.001
FFA	35.09	14.89	42.93	9.53	0.274
LPC	0.95	0.17	3.11	0.67	<0.001
LPE	0.66	0.13	4.67	0.91	<0.001
LPI	0.08	0.03	0.08	0.03	0.631
PC	98.77	18.06	125.51	18.44	0.025
PC-P	0.01	0.01	1.28	0.30	<0.001
PE	44.47	10.33	66.49	10.50	0.003
PE-P	0.12	0.04	6.39	1.44	<0.001
PG	1.07	0.34	4.92	1.25	<0.001
PI	10.43	3.12	11.11	1.95	0.631
PS	2.55	0.33	4.97	0.44	<0.001
PS-P	0.16	0.08	0.22	0.10	0.191
SM	0.63	0.22	1.07	0.50	0.076
TG	13.83	3.56	11.28	1.33	0.109

Data are presented as means  $\pm$  SD;  $n = 7$  for liver and  $n = 8$  for muscle mitochondria. The Response Screening platform in JMP 13.0 (SAS, Cary, NC) was used, considering a false discovery rate (FDR) *P* value < 0.05 as significant. CER, ceramides; CL, cardiolipins; FFA, free fatty acid; LPC, lysophosphatidylcholines; LPE, lysophosphatidylethanolamines; LPI, lysophosphatidylinositols; PC, phosphatidylcholines; PC-P, phosphatidylcholine plasmalogens; PE, phosphatidylethanolamines; PE-P, phosphatidylethanolamine plasmalogens; PG, phosphatidylglycerols; PI, phosphatidylinositols; PL, total phospholipids; PS, phosphatidylserines; PS-P, phosphatidylserine plasmalogens; SM, sphingomyelins; TG, triacylglycerols.

dria showed high respiration on complex I-linked substrates pyruvate and glutamate, whereas liver mitochondria respired less on these substrates but showed high respiration on complex II-linked substrate succinate. Our detailed investigation of the tissue-specific respiration on the substrates pyruvate, glutamate, succinate, and octanoylcarnitine extend previous reports obtained with isolated mitochondria of a type 2 diabetes rat model (Goto-Kakizaki rats) and whole muscle and liver tissue from mice (16, 21). Moreover, the integration of proteomics and lipidomics analyses underlines these divergent metabolic activities of muscle and liver mitochondria and highlights the molecular determinants.

The enzymes responsible for the different metabolic routes of pyruvate in mitochondria showed a tissue-specific distribution. Complex I-linked substrate pyruvate can be shuttled into different metabolic routes in mitochondria. After conversion to acetyl-CoA by pyruvate dehydrogenase complex, it is further oxidized in the TCA cycle, thereby feeding electrons into the respiratory chain. Acetyl-CoA is also shuttled into anabolic pathways (e.g., ketogenesis, fatty acid synthesis). Pyruvate can also be metabolized to oxaloacetate by pyruvate carboxylase, which is then used for gluconeogenesis. Proteins of the pyruvate dehydrogenase complex were found to be higher in muscle lysates and muscle mitochondria. Citrate synthase, which catalyzes the entry of acetyl-CoA into the TCA cycle by condensating it with oxaloacetate to citrate, was highly abundant in muscle tissue and mitochondria compared with liver. In contrast, we detected almost no pyruvate carboxylase in muscle tissue and mitochondria, whereas it was prominently detected in liver, the main site for gluconeogenesis. Additionally, ketogenic enzymes were highly abundant in liver mitochondria

but not in muscle. These results clearly indicate that in muscle, pyruvate is mainly used for complex I-dependent ATP production, whereas in liver mitochondria it serves as substrate for gluconeogenesis and ketogenesis. The other used complex I-linked substrate glutamate enters the TCA cycle as  $\alpha$ -ketoglutarate, a step catalyzed by glutamate dehydrogenase, thereby producing NADH. Notably, even though glutamate dehydrogenase was the fifth most abundant protein in liver mitochondria, only a low increase in  $\text{O}_2$  flux after glutamate addition was detected in liver mitochondria. This indicates that feeding electrons via complex I into the electron transport chain has a low capacity in liver mitochondria, whereas in skeletal muscle it is the preferred entry. In contrast, electrons delivered via complex II from oxidation of succinate or via electron transfer flavoproteins from  $\beta$ -oxidation to ubiquinone strongly activate respiration of liver mitochondria.

The tissue specificity of the mitochondrial respiratory complexes detected in our study and in part described in previous reports (10, 38) further substantiated the differences in respiration. Muscle mitochondria are characterized by a higher contribution of almost all subunits of complex I to the total proteome compared with liver and a higher contribution of most subunits of complex III, IV, and ATP synthase. The higher phosphorylating respiration in liver mitochondria after the addition of the complex II-linked substrate succinate is apparently not based on differences in the abundance of complex II subunits, since only SDHA showed higher abundance in liver mitochondria, whereas SDHB and SDHC were higher in muscle. However, the two most abundant SDH assembly factors SDHF 1 and 2 were higher in liver mitochondria (Supplemental Material B is available at <https://doi.org/10.6084/m9.figshare.7993766.v1>). These are necessary for maturation and maintaining SDH activity (55). SDH activity is also necessary to shuttle the amino acids valine, isoleucine, methionine, and threonine toward gluconeogenesis. They are

Table 2. Membrane lipid class levels in isolated mitochondria from mouse liver and skeletal muscle as percentage of the total amount of the major membrane lipids (phospho- and sphingolipids)

Lipid Class	Mean Liver/ ML, %	SD Liver	Mean Muscle/ ML, %	SD Muscle	FDR <i>P</i> Value
CER	0.48	0.14	0.33	0.06	0.022
CL	6.90	0.74	11.86	0.96	<0.001
LPC	0.56	0.09	1.19	0.20	<0.001
LPE	0.39	0.05	1.80	0.38	<0.001
LPI	0.05	0.01	0.03	0.01	0.022
PC (incl. PC-P)	57.43	1.63	48.48	0.78	<0.001
PE (incl. PE-P)	25.70	1.09	27.80	0.67	0.001
PG	0.61	0.08	1.86	0.18	<0.001
PI	5.94	0.76	4.24	0.28	<0.001
PS (incl. PS-P)	1.59	0.21	2.00	0.11	0.001
SM	0.36	0.07	0.41	0.17	0.492

Data are presented as means  $\pm$  SD;  $n = 7$  for liver, and  $n = 8$  for muscle mitochondria. Statistical analysis was performed by JMP 13.0 (SAS, Cary, NC), considering a false discovery rate (FDR) *P* value < 0.05 as significant. CER, ceramides; CL, cardiolipins; LPC, lysophosphatidylcholines; LPE, lysophosphatidylethanolamines; LPI, lysophosphatidylinositols; ML, membrane lipid; PC, phosphatidylcholines; PC-P, phosphatidylcholine plasmalogens; PE, phosphatidylethanolamines; PE-P, phosphatidylethanolamine plasmalogens; PG, phosphatidylglycerols; PI, phosphatidylinositols; PL, total phospholipids; PS, phosphatidylserines; PS-P, phosphatidylserine plasmalogens; SM, sphingomyelins.

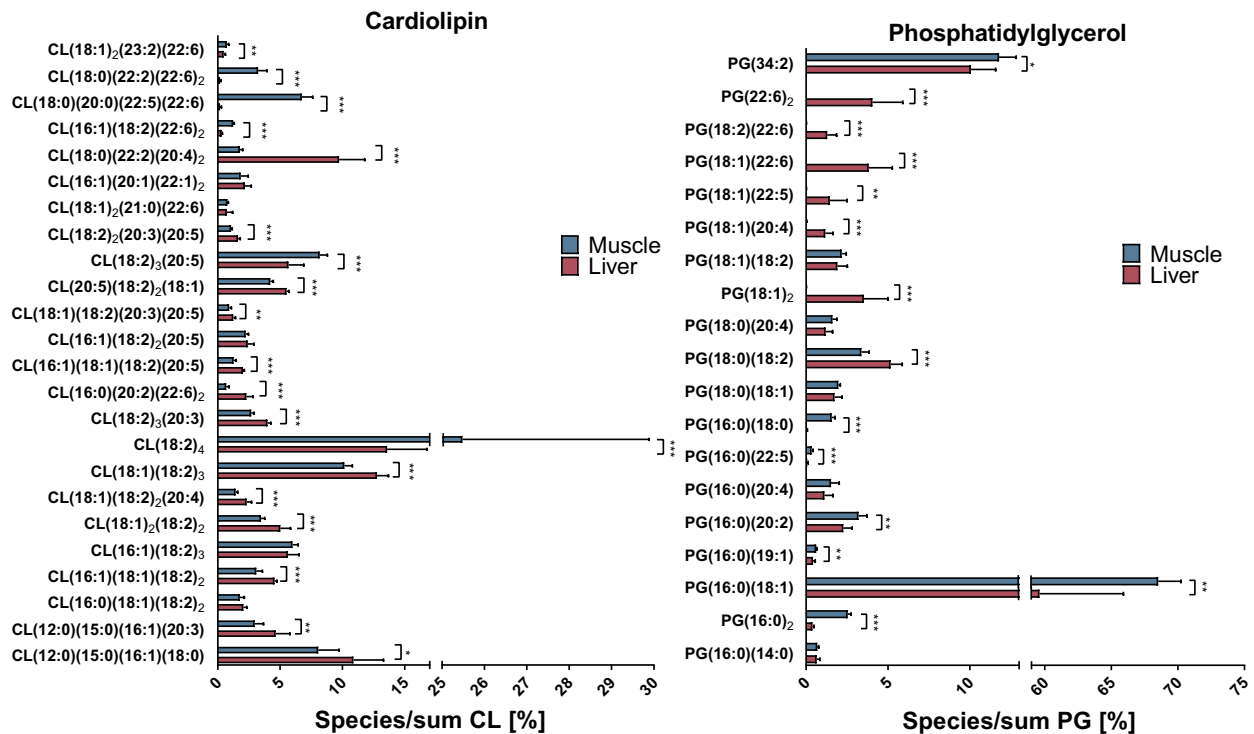


Fig. 6. Acyl chain patterns of mitochondrial cardiolipin (CL) and its precursor phosphatidylglycerol (PG) from isolated mouse skeletal muscle and liver mitochondria [ $n = 8$ , lipid content as percentage of the total CL (left) or PG (right) amount]. Data are presented as means  $\pm$  SD. The Response Screening platform in JMP 13.0 (SAS, Cary, NC) was used, considering a false discovery rate  $P$  value  $< 0.05$  as significant. \* $P < 0.05$ , \*\* $P < 0.01$ , \*\*\* $P < 0.001$ .

degraded to propionyl-CoA, which is converted to succinyl-CoA. The enzyme responsible for this last step, methylmalonyl-CoA mutase, was seven times more abundant in liver than in muscle mitochondria (Supplemental Material B). The proteome data also underline the preference of the liver to use fatty acids and branched-chain amino acids as substrates for oxidation and feeding electrons via  $FADH_2$  into the electron transport chain. This includes the higher abundance of enzymes involved in  $\beta$ -oxidation and branched-chain amino acid oxidation and the higher abundance of electron transfer flavoproteins ETFA, ETFB, and ETFD. Together, our data demonstrate the dominant function of muscle mitochondria to generate ATP, which is particularly needed during physical activity because of the high ATP consumption of the contracting muscle. Muscle tissue has not only a higher density of mitochondria (3) but also the muscle mitochondria are tailored to achieve a high capacity of oxidative phosphorylation. The preferred usage of complex I-linked substrates is of advantage as a more efficient way of electron transfer for ATP production, since all three proton-pumping complexes are involved. The high capacity of liver mitochondria for oxidation of succinate mirrors that SDH is not only required for feeding electrons into the electron transport chain but also to maintain gluconeogenesis.

Our data on mitochondrial phospholipid content and composition underline the tissue-specific different functions of muscle and liver mitochondria. We found that levels of the mitochondrial signature lipid CL, as well as its precursor PG, were significantly higher in mouse skeletal muscle. CLs are mainly located in the inner membrane of mitochondria (17), facilitating tight membrane folding and cristae formation (3, 41). CLs directly interact with respiratory chain complexes

(27, 58) and the ATP synthase (1), thereby regulating ATP production. Genetic disorders with impact on CL metabolism result in depleted CL levels and mitochondrial dysfunction such as Barth's syndrome and underscore the essential role of CL (31). Furthermore, CL is a critical component for stabilizing respiratory supercomplexes from complexes I, III, and IV, which in turn are thought to increase the

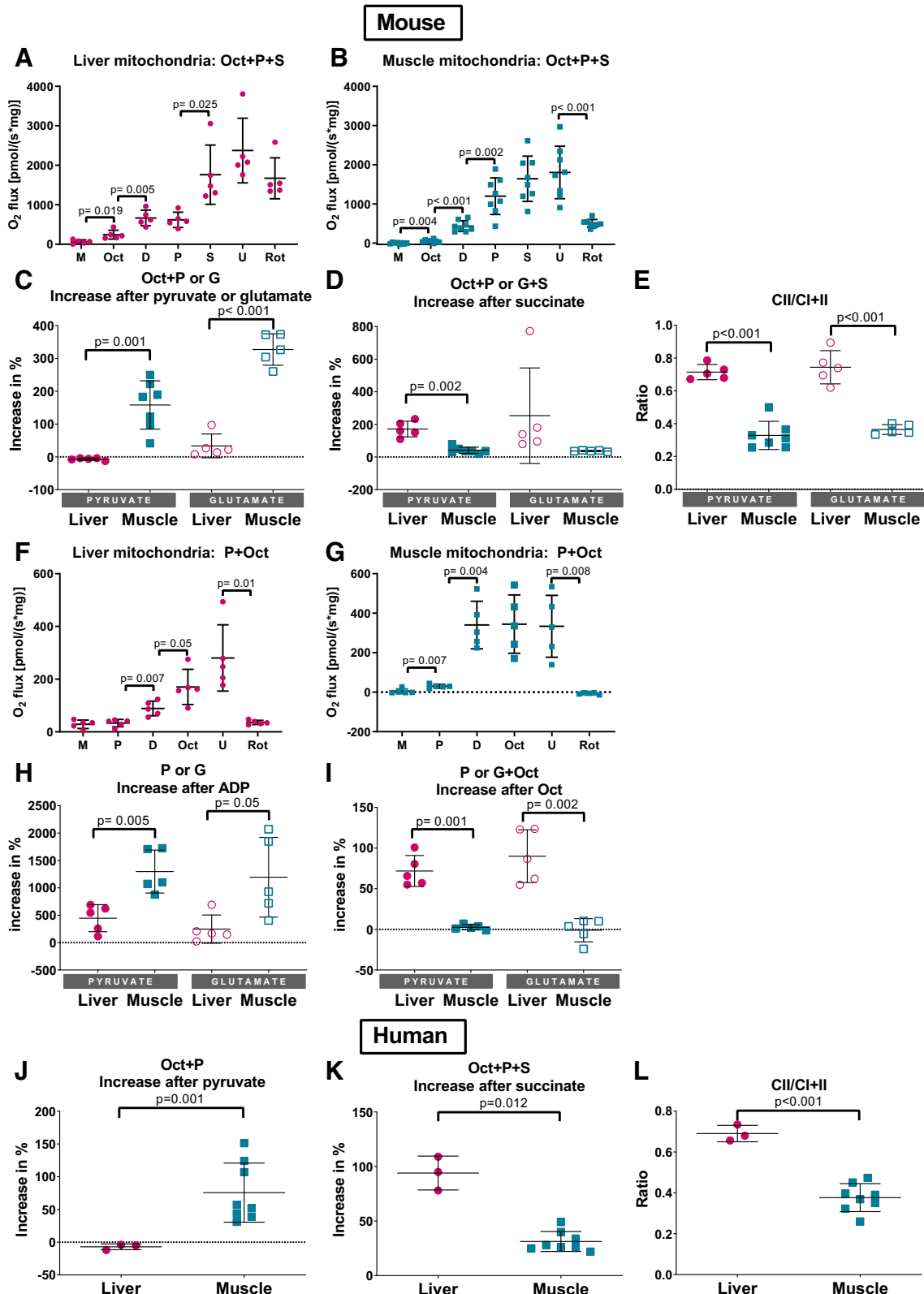
Table 3. Acyl chain composition of cardiolipins from mitochondria derived from mouse liver and muscle

FA	Liver, %	SD Liver	Muscle, %	SD Muscle	FDR $P$ Value
12:0	3.88	0.89	2.76	0.59	0.011
15:0	3.88	0.89	2.76	0.59	0.011
16:0	1.09	0.07	0.61	0.14	0.003
16:1	8.15	0.69	6.68	0.81	0.010
18:0	5.24	1.01	4.95	0.67	0.643
18:1	10.73	0.57	8.19	0.57	0.003
18:2	47.27	4.65	55.24	4.23	0.011
20:0	0.04	0.03	1.69	0.22	0.003
20:1	0.54	0.13	0.46	0.15	0.227
20:2	0.57	0.13	0.17	0.05	0.003
20:3	2.87	0.31	1.91	0.14	0.003
20:4	5.45	1.05	1.25	0.15	0.003
20:5	4.62	0.42	4.47	0.12	0.209
21:0	0.18	0.11	0.19	0.02	0.515
22:1	1.09	0.26	0.92	0.30	0.227
22:2	2.48	0.50	1.25	0.22	0.003
22:5	0.04	0.03	1.69	0.22	0.003
22:6	1.74	0.47	4.64	0.69	0.003
23:2	0.12	0.04	0.18	0.04	0.015

Data are presented as means  $\pm$  SD. Statistical analysis was performed by JMP 13.0 (SAS, Cary, NC), considering a false discovery rate (FDR)  $P$  value  $< 0.05$  as significant. FA, fatty acyl chain.

efficiency of electron transfer (26, 36). Thus, the higher content of CL found in muscle mitochondria is probably responsible for the higher density of cristae described for muscle mitochondria (3) and the higher capacity for super-

complex assembly including complex I (48, 58), both of which support ATP generation. Notably, exercise training has been shown to increase muscle CL content and super-complex formation (12, 32), underlining the importance of



CL for the high-oxidative phosphorylation capacity of the muscle.

CLs are glycerol-bridged, dimeric phospholipids substituted with four fatty acyl side chains, which opens up a huge number of possible molecular lipid species that have just started to be unraveled (29). The underlying process of CL remodeling is of extraordinary selectivity, exemplified by the detected differences in CL species in muscle and liver. Although 18:2 is the dominating acyl chain in both tissues, the relative amount of (18:2)<sub>4</sub>-CL is higher in muscle than in liver mitochondria, and this CL species has been associated with higher activity of respiratory complexes supporting our hypothesis of muscle mitochondria being more specified for oxidative phosphorylation than liver (9, 52). Lipidomics analysis of the specific CL side chain composition is the prerequisite for a better understanding of these molecular patterns and their possible impact on tissue-specific mitochondrial function, for example, the observed substrate preference of muscle and liver mitochondria. In skeletal muscle mitochondria, the second most abundant polyunsaturated fatty acid in CL was 22:6. CL containing 22:6 acyl chains might be essential to provide the high-oxidative phosphorylation flexibility in muscle mitochondria. This hypothesis is supported by an improved ADP sensitivity found in human skeletal muscle mitochondria with an increased 22:6 acyl chain content after dietary supplementation (15). Exercise training was also shown to increase 22:6 acyl chains in muscle phospholipids in mice and in humans (2, 50). In mouse heart, even more than 50% of all CL species contained 22:6 acyl chains (33). PE levels were also significantly higher in muscle than in liver mitochondria. This lipid class might also play a role in mitochondrial function, since a depletion of mitochondrial PE in cells led to defective electron transport chain complexes and a decreased respiratory capacity (54). Even though far from being completely understood, the tissue-specific lipid and acyl chain content of liver and muscle mitochondrial lipids presumably supports the adaptation to the different metabolic tasks of both tissues. The reported lipid patterns could be attributed very well to already published findings about lipids and their impact on mitochondrial function, but direct causalities for, e.g., specific CL species, can only be proven by using knockout models.

Our comparison of liver and muscle mitochondria is mainly based on using a mixture of upper hind limb muscles from mice. These muscles mainly represent fast type 2 fibers, whereas slow type 1 fibers are rare in mice and restricted to a few muscles such as the soleus (49). Thus, we cannot exclude that comparing liver mitochondria with slow muscle fiber-derived mitochondria would lead to different results. However,

we confirmed our results on substrate preference and different contribution of complex I and II to maximal respiration in liver tissue homogenates and muscle fibers from humans. Human vastus lateralis muscle contains both slow and fast fibers with similar distribution, and using this mixed fiber type led to similar results. This indicates that the tissue-specific differences in mitochondrial respiration are also present when comparing liver and mixed muscle fibers. Moreover, the tissue-specific differences were found not only in isolated mitochondria but also when the cellular localization and organization of mitochondria is preserved. Whereas the mice in our study were highly comparable because they had the same sex (male) and age, no sign of illness, and were housed under the same conditions and fed a standardized diet ad libitum, a limitation of the human liver and muscle samples was that they were not derived from the same individual and the donors differ in sex, eating condition, and health status. However, the organ-specific differences in complex I- and II-driven respiration are almost identical to data from mice and appear to be independent from sex, fasting, or health status. Together, our data suggest that these results are of relevance for human mitochondria from muscle and liver tissue. As a next step, it would be of great interest to compare subsarcolemmal and intermyofibrillar mitochondria of skeletal muscle using this comprehensive investigation of proteomics, lipidomics, and respiration data.

The tissue-specific differences in mitochondrial equipment and function could play a role in disease pathologies and form an essential basis for specified drug targeting. Metformin is one of the most common therapeutics for treating type 2 diabetes. A still widely proposed action of metformin is the inhibition of complex I in liver mitochondria, however, at millimolar concentrations (8, 37). Considering our findings that complex I-linked respiration in liver is of minor relevance, an inhibition thereof as explanation for the efficacy of metformin seems unlikely. Notably, very recent research highlighted alternative mechanisms of the action of metformin on hepatic gluconeogenesis as inhibition of glycerol-3-phosphate dehydrogenase (28) and inhibition of fructose-1,6-bisphosphatase (19). The attempts to identify the target of metformin illustrate how an advanced knowledge about mitochondria and their distinct tissue specificities can support drug development.

Following this line, liver and skeletal muscle mitochondria appear to have different capacities to compensate for the metabolic disturbances in obesity and diabetes. In skeletal muscle, some evidence points to a decreased mitochondrial function in diabetes (23, 34, 42). This is in contrast to an increased mitochondrial function in liver of patients who are

Fig. 7. Respiratory analyses of isolated mouse liver and skeletal muscle mitochondria (A–I) and human liver tissue homogenate and skeletal muscle fibers (J–L) on an Oxygraph-2k. Respiration of mouse liver and skeletal muscle mitochondria (A–E) with consecutive addition of malate (M), octanoylcarnitine (Oct), ADP (D), pyruvate (P), or glutamate (G) and succinate (S). Titration protocol, exemplarily shown for measurements with P (A and B). Increase of phosphorylating respiration with P or G (complex I substrates) (C). Increase of phosphorylating respiration with succinate (complex II substrate) (D). Ratio of maximal uncoupled complex II respiration to total maximal uncoupled respiration with complex I and II substrates;  $n = 5$  for liver mitochondria and  $n = 8$  for muscle mitochondria isolated from 8 mice (E). Respiration of mouse liver and skeletal muscle mitochondria with consecutive addition of M, P or G, D, and Oct as substrates (F–I). Titration protocol, exemplarily shown for P (F and G). Increase of respiration after ADP injection (H). Increase of phosphorylating respiration with Oct,  $n = 5$  for liver and muscle mitochondria isolated from 5 mice not identical with A–E (I); Titration protocol performed as shown in A and B with human liver tissue homogenate (3 donors) and skeletal muscle fibers (8 donors) (J–L); Increase of phosphorylating respiration with P (J). Increase of phosphorylating respiration with S (K). Ratio of maximal uncoupled complex II respiration to total maximal uncoupled respiration with complex I and II substrates (L). Data are presented as means  $\pm$  SD. Statistical significance was evaluated by Student's *t*-test. Rot, rotenone (complex I inhibitor); U, uncoupled respiration using the protonophore carbonylcyanide *p*-trifluoromethoxyphenylhydrazine.

insulin resistant, have diabetes, or have nonalcoholic fatty liver disease (24, 53). Future research will show whether some of the observed tissue-specific differences play a role in this different adaptation of muscle and liver mitochondria to insulin resistance and diabetes.

In conclusion, we present a comprehensive investigation of isolated mitochondria from mouse skeletal muscle and liver covering not only molecular but also functional analyses to obtain tissue-specific protein and lipid profiles and the consequences for respiration. In muscle mitochondria, we found a high contribution of respiratory complex I, III, IV, and ATP synthase subunits to the mitochondrial proteome and a high content of CL, in particular of (18:2)<sub>4</sub>-CL and 22:6 containing CL, in accordance with the high specialization of these mitochondria to rapidly and drastically increase the rate of ATP production whenever necessary. On the other hand, liver mitochondria are adapted to generate metabolites for biosynthetic pathways of gluconeogenesis and ketogenesis while relying on fatty acids and amino acids for oxidative phosphorylation. The results can build the base for a deeper understanding of mitochondrial function and dysfunction in states of health or disease by providing a global coverage of mitochondria. The investigation of tissue specificities of mitochondria might also help to interpret the often controversial findings in mitochondrial research. Thus, our data show how mitochondria are specialized in a tissue-specific fashion to ensure efficient utilization of available substrates.

#### ACKNOWLEDGMENTS

The authors are grateful for the excellent technical support provided by Heike Runge from the University Hospital Tübingen, Tübingen, Germany.

#### GRANTS

J. Li was supported by a research fellow grant of the Alexander von Humboldt Foundation. We gratefully acknowledge the financial support from the German Federal Ministry of Education and Research (BMBF) to the German Centre for Diabetes Research (Grant no. 01GI0925), from the National Key Research and Development Program of China (Grant no. 2017YFC0906900), and the National Natural Science Foundation of China (Grant nos. 21874130 and 21435006) to G. Xu, and the support by the Ministerium für Kultur und Wissenschaft des Landes Nordrhein-Westfalen, the Regierende Bürgermeister von Berlin - inkl. Wissenschaft und Forschung, and the BMBF (to L. Kollipara and A. Sickmann).

#### DISCLOSURES

No conflicts of interest, financial or otherwise, are declared by the authors.

#### AUTHOR CONTRIBUTIONS

L. Kappler, M.H., and C.W. conceived and designed research; L. Kappler, M.H., C. Hu, C.v.T., J.L., D.B., C. Hoffmann, and A.B. performed experiments; L. Kappler, C. Hu, A.S., and S.M.H. analyzed data; L. Kappler, M.H., C.W., and R.L. interpreted results of experiments; L. Kappler prepared figures; L. Kappler drafted manuscript; L. Kappler, M.H., H.-U.H., G.X., C.W., and R.L. edited and revised manuscript; L. Kappler, M.H., C. Hu, C.v.T., J.L., D.B., C. Hoffmann, A.B., L. Kollipara, H.Z., A.K., H.-U.H., A.P., G.X., A.S., S.M.H., C.W., and R.L. approved final version of manuscript.

#### REFERENCES

- Acehan D, Malhotra A, Xu Y, Ren M, Stokes DL, Schlame M. Cardiolipin affects the supramolecular organization of ATP synthase in mitochondria. *Biophys J* 100: 2184–2192, 2011. doi:10.1016/j.bpj.2011.03.031.
- Andersson A, Sjödin A, Hedman A, Olsson R, Vessby B. Fatty acid profile of skeletal muscle phospholipids in trained and untrained young men. *Am J Physiol Endocrinol Metab* 279: E744–E751, 2000. doi:10.1152/ajpendo.2000.279.4.E744.
- Benard G, Faustin B, Passerieux E, Galinier A, Rocher C, Bellance N, Delage J-P, Casteilla L, Letellier T, Rossignol R. Physiological diversity of mitochondrial oxidative phosphorylation. *Am J Physiol Cell Physiol* 291: C1172–C1182, 2006. doi:10.1152/ajpcell.00195.2006.
- Bloemberg D, Quadriatero J. Rapid determination of myosin heavy chain expression in rat, mouse, and human skeletal muscle using multi-color immunofluorescence analysis. *PLoS One* 7: e35273, 2012. doi:10.1371/journal.pone.0035273.
- Chen S, Hoene M, Li J, Li Y, Zhao X, Häring HU, Schleicher ED, Weigert C, Xu G, Lehmann R. Simultaneous extraction of metabolome and lipidome with methyl tert-butyl ether from a single small tissue sample for ultra-high performance liquid chromatography/mass spectrometry. *J Chromatogr A* 1298: 9–16, 2013. doi:10.1016/j.chroma.2013.05.019.
- Claypool SM. Cardiolipin, a critical determinant of mitochondrial carrier protein assembly and function. *Biochim Biophys Acta* 1788: 2059–2068, 2009. doi:10.1016/j.bbame.2009.04.020.
- DeFronzo RA, Jacot E, Jequier E, Maeder E, Wahren J, Felber JP. The effect of insulin on the disposal of intravenous glucose. Results from indirect calorimetry and hepatic and femoral venous catheterization. *Diabetes* 30: 1000–1007, 1981. doi:10.2337/diab.30.12.1000.
- El-Mir MY, Nogueira V, Fontaine E, Avéret N, Rigoulet M, Leverve X. Dimethylbiguanide inhibits cell respiration via an indirect effect targeted on the respiratory chain complex I. *J Biol Chem* 275: 223–228, 2000. doi:10.1074/jbc.275.1.223.
- Fajardo VA, McMeekin L, Saint C, LeBlanc PJ. Cardiolipin linoleic acid content and mitochondrial cytochrome c oxidase activity are associated in rat skeletal muscle. *Chem Phys Lipids* 187: 50–55, 2015. doi:10.1016/j.chemphyslip.2015.02.004.
- Forner F, Foster LJ, Campanaro S, Valle G, Mann M. Quantitative proteomic comparison of rat mitochondria from muscle, heart, and liver. *Mol Cell Proteomics* 5: 608–619, 2006. doi:10.1074/mcp.M500298-MCP200.
- Furler SM, Cooney GJ, Hegarty BD, Lim-Fraser MY, Kraegen EW, Oakes ND. Local factors modulate tissue-specific NEFA utilization: assessment in rats using 3H-(R)-2-bromopalmitate. *Diabetes* 49: 1427–1433, 2000. doi:10.2337/diabetes.49.9.1427.
- Greggio C, Jha P, Kulkarni SS, Lagarrigue S, Broskey NT, Boutant M, Wang X, Conde Alonso S, Ofori E, Auwerx J, Cantó C, Amati F. Enhanced respiratory chain supercomplex formation in response to exercise in human skeletal muscle. *Cell Metab* 25: 301–311, 2017. doi:10.1016/j.cmet.2016.11.004.
- Grosche A, Hauser A, Lepper MF, Mayo R, von Toerne C, Merl-Pham J, Hauck SM. The proteome of native adult Müller glial cells from murine retina. *Mol Cell Proteomics* 15: 462–480, 2016. doi:10.1074/mcp.M115.052183.
- Heden TD, Neuffer PD, Funai K. Looking beyond structure: membrane phospholipids of skeletal muscle mitochondria. *Trends Endocrinol Metab* 27: 553–562, 2016. doi:10.1016/j.tem.2016.05.007.
- Herbst EA, Paglialunga S, Gerling C, Whitfield J, Mukai K, Chabowski A, Heigenhauser GJ, Spriet LL, Holloway GP. Omega-3 supplementation alters mitochondrial membrane composition and respiration kinetics in human skeletal muscle. *J Physiol* 592: 1341–1352, 2014. doi:10.1113/jphysiol.2013.267336.
- Holmström MH, Iglesias-Gutierrez E, Zierath JR, Garcia-Roves PM. Tissue-specific control of mitochondrial respiration in obesity-related insulin resistance and diabetes. *Am J Physiol Endocrinol Metab* 302: E731–E739, 2012. doi:10.1152/ajpendo.00159.2011.
- Horvath SE, Daum G. Lipids of mitochondria. *Prog Lipid Res* 52: 590–614, 2013. doi:10.1016/j.plipres.2013.07.002.
- Hu A, Noble WS, Wolf-Yadlin A. Technical advances in proteomics: new developments in data-independent acquisition. *F1000 Res* 5: 419, 2016. doi:10.12688/f1000research.7042.1.
- Hunter RW, Hughey CC, Lantier L, Sundelin EI, Peggie M, Zeqiraj E, Sicheri F, Jessen N, Wasserman DH, Sakamoto K. Metformin reduces liver glucose production by inhibition of fructose-1-6-bisphosphatase. *Nat Med* 24: 1395–1406, 2018. doi:10.1038/s41591-018-0159-7.
- Johnson DT, Harris RA, French S, Blair PV, You J, Bemis KG, Wang M, Balaban RS. Tissue heterogeneity of the mammalian mitochondrial proteome. *Am J Physiol Cell Physiol* 292: C689–C697, 2007. doi:10.1152/ajpcell.00108.2006.
- Jørgensen W, Jølnes P, Rud KA, Hansen LL, Grønnet N, Quistorff B. Progression of type 2 diabetes in GK rats affects muscle and liver mitochondria.

- dria differently: pronounced reduction of complex II flux is observed in liver only. *Am J Physiol Endocrinol Metab* 303: E515–E523, 2012. doi:10.1152/ajpendo.00103.2012.
22. Kappler L, Li J, Häring HU, Weigert C, Lehmann R, Xu G, Hoene M. Purity matters: A workflow for the valid high-resolution lipid profiling of mitochondria from cell culture samples. *Sci Rep* 6: 21107, 2016. doi:10.1038/srep21107.
  23. Kelley DE, He J, Menshikova EV, Ritov VB. Dysfunction of mitochondria in human skeletal muscle in type 2 diabetes. *Diabetes* 51: 2944–2950, 2002. doi:10.2337/diabetes.51.10.2944.
  24. Koliaki C, Szendroedi J, Kaul K, Jelenik T, Nowotny P, Jankowiak F, Herder C, Carstensen M, Krausch M, Knoefel WT, Schlensak M, Roden M. Adaptation of hepatic mitochondrial function in humans with non-alcoholic fatty liver is lost in steatohepatitis. *Cell Metab* 21: 739–746, 2015. doi:10.1016/j.cmet.2015.04.004.
  25. Lanza IR, Sreekumar Nair K. Regulation of skeletal muscle mitochondrial function: genes to proteins. *Acta Physiol (Oxf)* 199: 529–547, 2010. doi:10.1111/j.1748-1716.2010.02124.x.
  26. Lapuente-Brun E, Moreno-Loshuertos R, Acín-Pérez R, Latorre-Pellicer A, Colás C, Balsa E, Perales-Clemente E, Quirós PM, Calvo E, Rodríguez-Hernández MA, Navas P, Cruz R, Carracedo Á, López-Otín C, Pérez-Martos A, Fernández-Silva P, Fernández-Vizarra E, Enriquez JA. Supercomplex assembly determines electron flux in the mitochondrial electron transport chain. *Science* 340: 1567–1570, 2013. doi:10.1126/science.1230381.
  27. Lee Y, Willers C, Kunji ERS, Crichton PG. Uncoupling protein 1 binds one nucleotide per monomer and is stabilized by tightly bound cardiolipin. *Proc Natl Acad Sci USA* 112: 6973–6978, 2015. doi:10.1073/pnas.1503833112.
  28. Madiraju AK, Erion DM, Rahimi Y, Zhang X-M, Braddock DT, Albright RA, Prigaro BJ, Wood JL, Bhanot S, MacDonald MJ, Jurczak MJ, Camporez JP, Lee H-Y, Cline GW, Samuel VT, Kibbey RG, Shulman GI. Metformin suppresses gluconeogenesis by inhibiting mitochondrial glycerophosphate dehydrogenase. *Nature* 510: 542–546, 2014. doi:10.1038/nature13270.
  29. Maguire JJ, Tyurina YY, Mohammadyani D, Kapralov AA, Anthony-muthu TS, Qu F, Amoscato AA, Sparvero LJ, Tyurin VA, Planas-Iglesias J, He RR, Klein-Seetharaman J, Bayir H, Kagan VE. Known unknowns of cardiolipin signaling: the best is yet to come. *Biochim Biophys Acta Mol Cell Biol Lipids* 1862: 8–24, 2017. doi:10.1016/j.bbalip.2016.08.001.
  30. McGarry JD, Foster DW. Regulation of hepatic fatty acid oxidation and ketone body production. *Annu Rev Biochem* 49: 395–420, 1980. doi:10.1146/annurev.bi.49.070180.002143.
  31. McKenzie M, Lazarou M, Thorburn DR, Ryan MT. Mitochondrial respiratory chain supercomplexes are destabilized in Barth Syndrome patients. *J Mol Biol* 361: 462–469, 2006. doi:10.1016/j.jmb.2006.06.057.
  32. Menshikova EV, Ritov VB, Dube JJ, Amati F, Stefanovic-Racic M, Toledo FGS, Coen PM, Goodpaster BH. Calorie restriction-induced weight loss and exercise have differential effects on skeletal muscle mitochondria despite similar effects on insulin sensitivity. *J Gerontol A Biol Sci Med Sci* 73: 81–87, 2017. doi:10.1093/gerona/glw328.
  33. Minkler PE, Hoppel CL. Separation and characterization of cardiolipin molecular species by reverse-phase ion pair high-performance liquid chromatography-mass spectrometry. *J Lipid Res* 51: 856–865, 2010. doi:10.1194/jlr.D002857.
  34. Mogensen M, Sahlin K, Fernström M, Glinborg D, Vind BF, Beck-Nielsen H, Højlund K. Mitochondrial respiration is decreased in skeletal muscle of patients with type 2 diabetes. *Diabetes* 56: 1592–1599, 2007. doi:10.2337/db06-0981.
  35. Mootha VK, Bunkenborg J, Olsen JV, Hjerrild M, Wisniewski JR, Stahl E, Bolouri MS, Ray HN, Sihag S, Kamal M, Patterson N, Lander ES, Mann M. Integrated analysis of protein composition, tissue diversity, and gene regulation in mouse mitochondria. *Cell* 115: 629–640, 2003. doi:10.1016/S0092-8674(03)00926-7.
  36. Osman C, Voelker DR, Langer T. Making heads or tails of phospholipids in mitochondria. *J Cell Biol* 192: 7–16, 2011. doi:10.1083/jcb.201006159.
  37. Owen MR, Doran E, Halestrap AP. Evidence that metformin exerts its anti-diabetic effects through inhibition of complex I of the mitochondrial respiratory chain. *Biochem J* 348: 607–614, 2000. doi:10.1042/bj3480607.
  38. Pagliarini DJ, Calvo SE, Chang B, Sheth SA, Vafai SB, Ong SE, Walford GA, Sugiana C, Boneh A, Chen WK, Hill DE, Vidal M, Evans JG, Thorburn DR, Carr SA, Mootha VK. A mitochondrial protein compendium elucidates complex I disease biology. *Cell* 134: 112–123, 2008. doi:10.1016/j.cell.2008.06.016.
  39. Pearce J. Fatty acid synthesis in liver and adipose tissue. *Proc Nutr Soc* 42: 263–271, 1983. doi:10.1079/PNS19830031.
  40. Pesta D, Gnaiger E. High-resolution respirometry: OXPHOS protocols for human cells and permeabilized fibers from small biopsies of human muscle. *Methods Mol Biol* 810: 25–58, 2012. doi:10.1007/978-1-61779-382-0\_3.
  41. Phan MD, Shin K. Effects of cardiolipin on membrane morphology: a Langmuir monolayer study. *Biophys J* 108: 1977–1986, 2015. doi:10.1016/j.bpj.2015.03.026.
  42. Phielix E, Schrauwen-Hinderling VB, Mensink M, Lenaers E, Meex R, Hoeks J, Kooi ME, Moonen-Kornips E, Sels JP, Hesselink MK, Schrauwen P. Lower intrinsic ADP-stimulated mitochondrial respiration underlies in vivo mitochondrial dysfunction in muscle of male type 2 diabetic patients. *Diabetes* 57: 2943–2949, 2008. doi:10.2337/db08-0391.
  43. Postic C, Dentin R, Girard J. Role of the liver in the control of carbohydrate and lipid homeostasis. *Diabetes Metab* 30: 398–408, 2004. doi:10.1016/S1262-3636(07)70133-7.
  44. Reiter L, Rinner O, Picotti P, Hüttenhain R, Beck M, Brusniak MY, Hengartner MO, Aebersold R. mProphet: automated data processing and statistical validation for large-scale SRM experiments. *Nat Methods* 8: 430–435, 2011. doi:10.1038/nmeth.1584.
  45. Rothman DL, Magnusson I, Katz LD, Shulman RG, Shulman GI. Quantitation of hepatic glycogenolysis and gluconeogenesis in fasting humans with <sup>13</sup>C NMR. *Science* 254: 573–576, 1991. doi:10.1126/science.1948033.
  46. Saeed AI, Sharov V, White J, Li J, Liang W, Bhagabati N, Braisted J, Klapa M, Currier T, Thiagarajan M, Sturn A, Snuffin M, Rezantsev A, Popov D, Ryltsov A, Kostukovich E, Borisovsky I, Liu Z, Vinsavich A, Trush V, Quackenbush J. TM4: a free, open-source system for microarray data management and analysis. *Biotechniques* 34: 374–378, 2003. doi:10.2144/03342mt01.
  47. Sajic T, Liu Y, Aebersold R. Using data-independent, high-resolution mass spectrometry in protein biomarker research: perspectives and clinical applications. *Proteomics Clin Appl* 9: 307–321, 2015. doi:10.1002/prca.201400117.
  48. Schägger H, Pfeiffer K. Supercomplexes in the respiratory chains of yeast and mammalian mitochondria. *EMBO J* 19: 1777–1783, 2000. doi:10.1093/emboj/19.8.1777.
  49. Schiaffino S. Fibre types in skeletal muscle: a personal account. *Acta Physiol (Oxf)* 199: 451–463, 2010. doi:10.1111/j.1748-1716.2010.02130.x.
  50. Senoo N, Miyoshi N, Goto-Inoue N, Minami K, Yoshimura R, Morita A, Sawada N, Matsuda J, Ogawa Y, Setou M, Kamei Y, Miura S. PGC-1 $\alpha$ -mediated changes in phospholipid profiles of exercise-trained skeletal muscle. *J Lipid Res* 56: 2286–2296, 2015. doi:10.1194/jlr.M060533.
  51. Smith AC, Robinson AJ. MitoMiner v3.1, an update on the mitochondrial proteomics database. *Nucleic Acids Res* 44: D1258–D1261, 2016. doi:10.1093/nar/gkv1001.
  52. Sullivan EM, Pennington ER, Sparagna GC, Torres MJ, Neuffer PD, Harris M, Washington J, Anderson EJ, Zeczycki TN, Brown DA, Shaikh SR. Docosahexaenoic acid lowers cardiac mitochondrial enzyme activity by replacing linoleic acid in the phospholipidome. *J Biol Chem* 293: 466–483, 2018. doi:10.1074/jbc.M117.812834.
  53. Takamura T, Misu H, Matsuzawa-Nagata N, Sakurai M, Ota T, Shimizu A, Kurita S, Takeshita Y, Ando H, Honda M, Kaneko S. Obesity upregulates genes involved in oxidative phosphorylation in livers of diabetic patients. *Obesity (Silver Spring)* 16: 2601–2609, 2008. doi:10.1038/oby.2008.419.
  54. Tasseva G, Bai HD, Davidescu M, Haromy A, Michelakis E, Vance JE. Phosphatidylethanolamine deficiency in Mammalian mitochondria impairs oxidative phosphorylation and alters mitochondrial morphology. *J Biol Chem* 288: 4158–4173, 2013. doi:10.1074/jbc.M112.434183.
  55. Van Vranken JG, Na U, Winge DR, Rutter J. Protein-mediated assembly of succinate dehydrogenase and its cofactors. *Crit Rev Biochem Mol Biol* 50: 168–180, 2015. doi:10.3109/10409238.2014.990556.
  56. Wallace DC. Bioenergetic origins of complexity and disease. *Cold Spring Harb Symp Quant Biol* 76: 1–16, 2011. doi:10.1101/sqb.2011.76.010462.
  57. Wiśniewski JR, Zougman A, Nagaraj N, Mann M. Universal sample preparation method for proteome analysis. *Nat Methods* 6: 359–362, 2009. doi:10.1038/nmeth.1322.
  58. Zhang M, Mileykovskaya E, Dowhan W. Gluing the respiratory chain together. Cardiolipin is required for supercomplex formation in the inner mitochondrial membrane. *J Biol Chem* 277: 43553–43556, 2002. doi:10.1074/jbc.C200551200.